Vibrational Transition Current Density in (*S*)-Methyl Lactate: Visualizing the Origin of the Methine-Stretching Vibrational Circular Dichroism Intensity

Teresa B. Freedman,*,† Eunah Lee, and Laurence A. Nafie*,‡

Department of Chemistry, Syracuse University, Syracuse, New York 13244-4100

Received: February 10, 2000

Vibrational transition current density (TCD) plots for the methine stretch of (*S*)-methyl-d_3 lactate-Cd_3 in four conformations are presented. A vibrational TCD map is a vector-field plot over a grid of points of the integrand of the electronic contribution to the velocity-form electric dipole transition moment. TCD plots allow visualization of the flow of electron density produced by nuclear motion, which can be used to identify angular and circular charge flow leading to the electronic magnetic dipole transition moment contribution to vibrational circular dichroism (VCD). For the methine stretch in (*S*)-methyl-d_3 lactate-Cd_3, nuclear motion is largely confined to the two atoms of the methine bond, but the electron current density is distributed throughout the molecule. The methine-stretching VCD intensity calculated for the (*S*)-methyl-d_3 lactate-Cd_3 conformers is interpreted in terms of the relative contributions from the nuclear electric- and magnetic-dipole transition moments, and from linear electron charge flow, circular electron charge flow about carbon and oxygen centers, and angular charge flow across groups of atoms. In this example, we find no evidence to support the existence of vibrational ring currents through hydrogen bonds, as proposed earlier based on empirical evidence, although the empirical correlations of structure to VCD still hold for such intramolecularly hydrogen-bonded molecules.

Introduction

Vibrational circular dichroism (VCD) intensity is proportional to the rotational strength $R = \mathrm{Im}(\vec{\mu})_{01}\cdot(\vec{m})_{10}$, the scalar product of the electric dipole transition moment, $(\vec{\mu})_{01}$, originating from linear oscillation of charge, and the magnetic dipole transition moment, $(\vec{m})_{10}$, originating from circular oscillation of charge, generated by the nuclear vibrational motion.[1−3] Although vibrational circular dichroism (VCD) spectra can now be calculated fairly routinely, with good agreement to experiment,[4−7] the electronic motion from which the intensities are generated cannot be deduced from such calculations. We recently introduced a method for calculating and visualizing the flow of electron density produced by electronic excitation or nuclear motion, utilizing plots of electron transition current density (TCD) for electronic and vibrational transitions.[3,8−12] The TCD vector field, which is related to the integrand of the velocity-form electric dipole transition moment, gives the magnitude and direction of vibrationally generated electron density current at each point in space. In practice, this corresponds to a TCD vector at each electron density volume element in a grid of points encompassing a molecule. The nuclear current is visualized from nuclear-charge-weighted nuclear velocity vectors (equivalent to charge-weighted nuclear displacement vectors[1]) located at the nuclei. By contrast, density difference plots produce a scalar map for a vibrational transition, but no information on the current pathways leading to density depletion or enrichment. Similarly, atomic polar tensor and atomic axial tensor elements provide atomic contributions to infrared and vibrational circular dichroism (VCD) intensities;[1,2,13] these integrated quantities are derived from the charge flows arising from atom displacement, but do not provide details of the electron currents leading to these tensor elements.

Our first publications of TCD for electronic[9] and vibrational[10] transitions in formaldehyde and ethylene revealed how visualization of the current patterns calculated from a velocity (linear momentum) operator provides information on the magnetic dipole and electric quadrupole nature of the transitions, in addition to the electric dipole character. For these simple achiral molecules, we found that nuclear motion could generate circulatory electron current about carbon and oxygen nuclei, as well as electron density motion that generally followed the nuclear motion, including angular motion across groups of atoms when allowed by symmetry.[10] Local circulatory atomic currents represent a pure magnetic dipole effect, since this motion does not contribute to an electric dipole moment and does not lead to a change in electron density with nuclear motion. Thus, the current patterns calculated for a velocity operator also provide insight into the magnetic dipole character of the vibrational transition.

For a chiral molecule, nonzero VCD intensity results from net clockwise or counterclockwise current about the direction of the electric dipole transition moment. By viewing the components of the TCD and charge-weighted nuclear velocities perpendicular to the direction of the electric dipole transition moment, contributions to the magnetic dipole transition moment from the nuclear motion, from angular electron motion about groups of atoms and from circular electron motion about atomic centers can be identified. For four vibrations of a chiral molecule, (2*S*,3*S*)-oxirane-d_2, we showed how TCD plots provide insight into the origins of the electronic contributions to both infrared and VCD intensity.[12]

In this study, we demonstrate how TCD plots can be used to understand the differences in VCD intensity for a molecule in a variety of conformations. VCD is measured as the difference in absorbance or molar absorptivity for left and right circularly

* To whom correspondence should be addressed.
† Tel: 315-443-1134. Fax: 315-443-4070. E-mail: tbfreedm@syr.edu.
‡ Tel: 315-443-4109. Fax: 315-443-4070. E-mail: lnafie@syr.edu.

10.1021/jp0005470 CCC: $19.00
Published on Web 03/31/2000

SCHEME 1

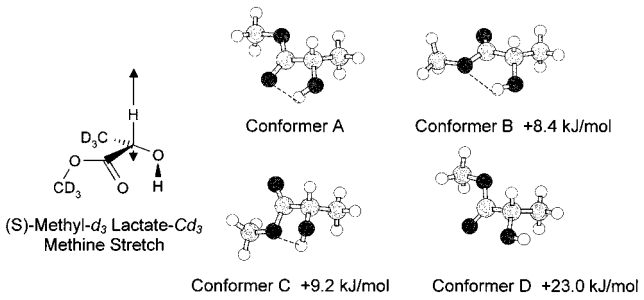

polarized infrared radiation, $\Delta\epsilon = \epsilon_L - \epsilon_R$. One of the largest VCD signals observed for an isolated nuclear motion is the methine stretch in amino acids,[14−16] methyl lactate,[4] and related molecules,[4,15,17] where the anisotropy ratio, $\Delta\epsilon/\epsilon$, is $2-4 \times 10^{-4}$. Based on the empirical correlation of large VCD intensity with the presence of a methine stretch adjacent to a hydrogen-bonded ring, a ring current mechanism for VCD was proposed a number of years ago, wherein the magnetic dipole moment content of the VCD intensity was postulated to arise from vibrationally generated electronic current about the hydrogen-bonded ring.[14,18,19] With the advent of a priori theoretical formalisms for VCD[20−24] and reliable ab initio molecular orbital implementations,[2,13,25,26] such descriptive models and mechanisms have been largely superseded by calculations of VCD intensity. For the methine stretch in methyl lactate, calculations showed that the VCD intensity for conformer D in Scheme 1, which has no hydrogen bond, is predicted to be fairly large and positive, only a factor of 2 smaller than for the most abundant conformer A, calling into question a premise of the ring current model.[4,27,28] Although conformer D is not populated in room temperature solution, we recently reported experimental evidence for a number of molecules related to methyl lactate (such as (*S*)-methyl-d_3 2-(methoxy-d_3)propionate) that correlates large methine stretching VCD with an O═C−C*−O dihedral angle near 0° and an O−O bond distance ∼2.7 Å, independent of any specific hydrogen-bonding interaction.[4] The origin of the magnetic dipole transition moment for the methine stretch in these molecules, including the specific role of the O═C−C*−O moiety and the importance of angular or circular electron charge flow involving such a moiety, thus remains an open question.

Theoretical Background

The integrated VCD intensity is proportional to the rotational or rotatory strength, the scalar product of the electric and magnetic dipole transition moments. In the harmonic approximation, the rotational strength is

$$R_{01}^{a} = \frac{\hbar}{2}\left(\frac{\partial\vec{\mu}_r}{\partial Q_a}\right)_0 \cdot \left(\frac{\partial\vec{m}}{\partial P_a}\right)_0 \tag{1}$$

where $\vec{\mu}_r$ is the position-form electric dipole moment of the molecule, $\vec{m}$ is the magnetic dipole moment of the molecule, and the derivatives are taken with respect to normal mode displacement Q_a or conjugate momentum P_a for normal mode a. The absorption intensity for the normal mode is given by the dipole strength, the square of the electric dipole transition moment, in the harmonic approximation expressed as

$$D_{01}^{a} = \frac{\hbar}{2\omega_a}\left|\left(\frac{\partial\vec{\mu}_r}{\partial Q_a}\right)_0\right|^2 \tag{2}$$

where ω_a is the angular frequency for mode a. A velocity formulation for the electric dipole transition moment can also be employed by utilizing the operator

$$\hat{\mu}_v = -\sum_j e\dot{\mathbf{r}}_j + \sum_J Z_J e\dot{\mathbf{R}}_J = \sum_j \frac{ie\hbar}{m}\frac{\partial}{\partial \mathbf{r}_j} - \sum_J \frac{ie\hbar Z_J}{M_J}\frac{\partial}{\partial \mathbf{R}_J} \tag{3}$$

for electrons j with mass m and charge $-e$ and nuclei J with mass M_J and charge $Z_J e$. The corresponding expressions for the velocity-form dipole and rotational strengths are obtained from the equality

$$\left(\frac{\partial\vec{\mu}_r}{\partial Q_a}\right)_0 = \left(\frac{\partial\vec{\mu}_v}{\partial P_a}\right)_0 \tag{4}$$

Although these two derivatives are formally equivalent, the electronic contribution to the velocity-form derivative requires correlation with nuclear velocities, and is a pure non-Born−Oppenheimer contribution, as is the electronic contribution to $(\partial\vec{m}/\partial P_a)_0$.[1,20,21]

As seen from eq 1, VCD intensity requires both vibrationally generated linear charge oscillation, $(\partial\vec{\mu}/\partial Q_a)_0$, and vibrationally generated circular or angular charge oscillation, $(\partial\vec{m}/\partial P_a)_0$, whereas dipole strength involves only linear charge flow (eq 2). In the past, numerous descriptive and calculational models for VCD have incorporated charge flow considerations to provide an understanding of the source of the intensity.[1] Use of these models has been largely replaced by comparison of observed data with ab initio molecular orbital calculations of VCD intensity derived from more exact a priori formulations.[2,13,26] Vibrational transition current density provides a way to employ these a priori formulations in a format that allows calculation and visualization of the charge flow produced by nuclear vibrational motion, thus providing insight into the origin of both IR and VCD intensity.

Plots of transition current density allow visualization of the flow of electron density during electronic or vibrational excitation. The electron transition current density for the e → s pure electronic transition is defined as[8]

$$\boldsymbol{J}_{es}^{0}(\mathbf{r}) = (\hbar/2m)[\psi_e^0\nabla\psi_s^0 - \psi_s^0\nabla\psi_e^0] \tag{5}$$

which is related to the integrand of the electronic contribution to the velocity form of the electric dipole transition moment:[8,9,20,21]

$$(\mu_v)_{es}^{E} = -\int \psi_e^0(\mathbf{r})e\dot{\mathbf{r}}\psi_s^0(\mathbf{r})\,d\mathbf{r} = -\int \psi_e^0(\mathbf{r})\left(\frac{-ie\hbar}{m}\nabla\right)\psi_s^0(\mathbf{r})\,d\mathbf{r} \tag{6}$$

$$= \frac{ie\hbar}{2m}\int[\psi_e^0(\mathbf{r})\nabla\psi_s^0(\mathbf{r}) - \psi_s^0(\mathbf{r})\nabla\psi_e^0(\mathbf{r})]\,d\mathbf{r} = -ie\int \boldsymbol{J}_{es}^{0}(\mathbf{r})\,d\mathbf{r} \tag{7}$$

For a vibrational transition, the vibrational transition current density is given by a sum over excited electronic states:

$$\boldsymbol{J}_{g0,g1}^{a}(\mathbf{r}) = 2i\sum_{s\neq g}\left[\frac{\left\langle\psi_s^0\left|\left(\frac{\partial\psi_g}{\partial Q_a}\right)_0\right\rangle\boldsymbol{J}_{gs}^{0}(\mathbf{r})}{\omega_{sg}^{0}}\right]\langle\phi_{g0}^{a}|P_a|\phi_{g1}^{a}\rangle = (2\hbar\omega_a)^{1/2}\sum_{s\neq g}\left[\frac{\left\langle\psi_s^0\left|\left(\frac{\partial\psi_g}{\partial Q_a}\right)_0\right\rangle\boldsymbol{J}_{gs}^{0}(\mathbf{r})}{\omega_{sg}^{0}}\right] \tag{8}$$

where ϕ^a_{g0} and ϕ^a_{g1} are the ground and excited state vibrational wave functions and ω^0_{sg} is the angular frequency difference between the excited and ground electronic states. The integrated form of $\boldsymbol{J}^a_{g0,g1}(\mathbf{r})$ is the electronic contribution to the velocity-form electric dipole transition moment for mode a in the non-Born−Oppenheimer sum-over-states vibronic coupling formulation.[1,20,21] Alternatively, eq 8 can be written as an expansion to first order in terms of the variation with P_a of the ground-state electron current density, $\boldsymbol{J}_g(\mathbf{r},P)$, which is zero in the absence of nuclear momentum, P_a, i.e., nuclear velocities.[21]

$$\boldsymbol{J}^a_{g0,g1}(\mathbf{r}) = \left(\frac{\partial \boldsymbol{J}_g(\mathbf{r},P)}{\partial P_a}\right)_0 \langle \phi^a_{g0}|P_a|\phi^a_{g1}\rangle \tag{9}$$

In utilizing TCD plots to visualize the origins of VCD intensity, it is useful to consider the expression for the rotational strength with locally distributed atomic origins[1]

$$(R^a_v)^{LDO} = \frac{\hbar}{2}\left[\sum_B \left(\frac{\partial \vec{\mu}^B_v}{\partial P_a}\right)_0\right]\cdot\left[\sum_{B'}\left\{\frac{1}{2c}\mathbf{R}^0_{B'}\times\left(\frac{\partial \vec{\mu}^{B'}_v}{\partial P_a}\right)_0 + \left(\frac{\partial \vec{m}^{B'}_{loc}}{\partial P_a}\right)_0\right\}\right] \tag{10}$$

In this case, the derivative of the velocity-form electric dipole moment is broken down into atomic contributions. This expression is exact, and origin independent, for the velocity-form dipole moment derivatives. In this expression, the derivative $(\partial \vec{m}/\partial P_a)_0$ (eq 1) includes contributions from two terms for each atom: a moment arm from the molecular origin to the atomic center crossed into the velocity-form electric dipole moment derivative atomic contribution, and a local intrinsic magnetic dipole moment term, centered at the atom, which involves an atomic magnetic moment operator. The nuclear contribution is contained in the first term

$$\mathbf{R}^0_B \times \left(\frac{\partial \vec{\mu}^B_v}{\partial P_a}\right)^{nuclear}_0 = \mathbf{R}^0_B \times \frac{Z_B e}{2c}\left(\frac{\partial \dot{\mathbf{R}}_B}{\partial P_a}\right)_0 = \mathbf{R}^0_B \times \frac{Z_B e}{2c}\left(\frac{\partial \mathbf{R}_B}{\partial Q_a}\right)_0 \tag{11}$$

where $Z_B e(\partial \mathbf{R}_B/\partial Q_a)_0$ is the charge-weighted displacement vector for atom B in normal mode a. In terms of the vibrational electron TCD vector field, $\boldsymbol{J}^a_{g0,g1}(\mathbf{r})$, the electronic contribution to the magnetic dipole transition moment $(\mathbf{m})^a_{01}$ is

$$[(\boldsymbol{m})^a_{01}]^{electronic} = [(\partial \vec{m}/\partial P_a)_0\langle \phi^a_{g0}|P_a|\phi^a_{g1}\rangle]^{electronic} = \frac{-ie}{2c}\int \mathbf{r}\times \boldsymbol{J}^a_{g0,g1}(\mathbf{r})\,d\mathbf{r} \tag{12}$$

This expression can also be broken down into atomic contributions, with $\boldsymbol{J}^a_{g0,g1}(\mathbf{r}) = \sum_B\{\boldsymbol{J}^a_{g0,g1}(\mathbf{r})\}^B$ and $\mathbf{r} = \boldsymbol{R}^0_B + \boldsymbol{r}_B$ (where the contribution from atom B to $\boldsymbol{J}^a_{g0,g1}(\mathbf{r})$ may be consistently defined, for example,[29] by utilizing only the atomic orbitals for atom B in the ground-state wave functions for $\boldsymbol{J}^0_{gs}(\mathbf{r})$ in eq 8:

$$[(\boldsymbol{m})^a_{01}]^{electronic} = \frac{-ie}{2c}\sum_B\left[\int \boldsymbol{R}^0_B \times \{\boldsymbol{J}^a_{g0,g1}(\mathbf{r})\}^B\,d\mathbf{r} + \int \boldsymbol{r}_B \times \{\boldsymbol{J}^a_{g0,g1}(\mathbf{r})\}^B\,d\mathbf{r}\right] \tag{13}$$

The atomic contributions $\{\boldsymbol{J}^a_{g0,g1}(\mathbf{r})\}^B$ are expected to fall off rapidly from atom B. With vibrational TCD maps, we consider the velocity-form electric dipole moment derivative contribution at each point of the grid (in contrast to integrated atomic contributions in eq 10). For the present application, the decomposition to atomic contributions will be made visually by looking for linear or circular TCD flow patterns in the vicinity of each atom. We then visually take cross products with a moment arm from a molecular origin at the center of mass to local regions of linear flow to identify angular charge flow about a group of atoms (first term in eq 13) or with a moment arm from an atomic origin to local circular current about an atomic center (second term in eq 13). The TCD current patterns can thus be related to electronic magnetic dipole transition moment contributions through eqs 12 or 13.

We have implemented the calculation of vibrational TCD as a sum-over-states calculation employing the single electron transition approximation for each ground to excited state pair in the sum.[10] The vectors $\boldsymbol{J}^a_{g0,g1}(\mathbf{r})$ are calculated over a grid of points[9] by employing a modification of the link in Gaussian 92[30] for calculating molecular orbitals, electron density, and density gradient over a three-dimensional grid, coupled to code adapted from our sum-over-states vibronic coupling calculations of VCD intensity,[1,20] which employs output from a Gaussian 94[31] or Gaussian 98[32] calculation. Visualization of the vibrational TCD vector field is achieved by employing the AVS visualization software (Advanced Visual Systems, Burlington, MA), with 3D presentation or 2D projections of TCD vectors superimposed on ball-and-stick or wire-frame models of the molecular structure and the nuclear displacement vectors.

(*S*)-Methyl Lactate Methine Stretch VCD

The methine-stretching mode serves as a marker for absolute configuration and solution conformation in amino acids,[14−16] peptides,[16] and α-hydroxy acids.[4] In a study of methyl lactate and related molecules,[4] we measured anisotropy ratios ($g = \Delta A/A = 4R/D$) for the methine stretches between 2.1×10^{-4} and 2.8×10^{-4}, some of the largest values observed for a mode with a single local oscillator, which correlates with a nearly planar, cis arrangement of the O═C−C*−O atoms encompassing the chiral center. VCD intensity calculations[4] utilizing the sum-over-states vibronic coupling (VCT) approach[20,25] reproduced the observed anisotropy ratio for (*S*)-methyl-d_3 lactate within a factor of 2 ($g_{obs} = 2.1 \times 10^{-4}$; $g_{calc} = 1.1 \times 10^{-4}$) for the lowest energy, OH- -O═C hydrogen-bonded conformer A, shown in Scheme 1. For conformer B, with an OH- -O(CH_3) hydrogen bond and trans arrangement of O═C−C*−O, a much smaller rotational strength and anisotropy ratio ($g = 0.1 \times 10^{-4}$) were calculated. The second OH- -O(CH_3) hydrogen-bonded conformer C also was calculated to have a large positive anisotropy ratio for the methine stretch ($g = 1.2 \times 10^{-4}$), whereas for the highest energy conformer D with a cis O═C−C*−O geometry, but no hydrogen bond, the calculated anisotropy ratio was half that of A ($g = 0.6 \times 10^{-4}$). The calculations for these anisotropy ratios were carried out for the isotopomers with both methyl groups deuterated [(*S*)-methyl-d_3 lactate-Cd_3], for which the methine-stretching normal mode is a highly localized, uncoupled C*H elongation, whereas the experimental measurement is for (*S*)-methyl-d_3 lactate, ~90% conformer A, and includes the effect of a small contribution from coupling with antisymmetric methyl deformation. A Hartree−Fock calculation of geometries, force field, and atomic polar tensors with a 6-31G$^{(0.3)}$ basis set was employed.[2,33] This basis set, based on 6-31G(d) with the d-orbital exponent reduced from 0.8 to 0.3 for second-row atoms, has been found to produce VCD intensities in good agreement with experiment for the VCT sum-over-states method for calculating VCD intensities.[2,7,33,34] The VCD spectra for the CH-stretching region of (*S*)-methyl-d_3

TABLE 1: Calculated Energies, Intensities, and Dipole Transition Moment *z*-Component Contributions for the Methine Elongation in Methyl-d_3 Lactate-Cd_3 Conformers

property	conformer A	conformer B	conformer C	conformer D
relative energy (kJ/mol)	0.0	+8.4	+9.2	+23.0
dipole strength (10^{-40} esu^2 cm^2)	33.7	42.7	14.8	39.0
rotational strength (10^{-45} esu^2 cm^2)	+90.7	+11.9	+43.6	+57.5
total μ_z^T (atomic units)	+0.165	+0.185	+0.111	+0.178
electronic μ_z^E (atomic units)	+0.612	+0.638	+0.569	+0.633
nuclear μ_z^N (atomic units)	−0.447	−0.453	−0.458	−0.455
total m_z^T (atomic units)	+0.085	+0.010	+0.061	+0.050
electronic m_z^E (DO gauge, atomic units)	−0.003	−0.179	−0.067	−0.029
nuclear m_z^N (atomic units)	+0.088	+0.189	+0.128	+0.079

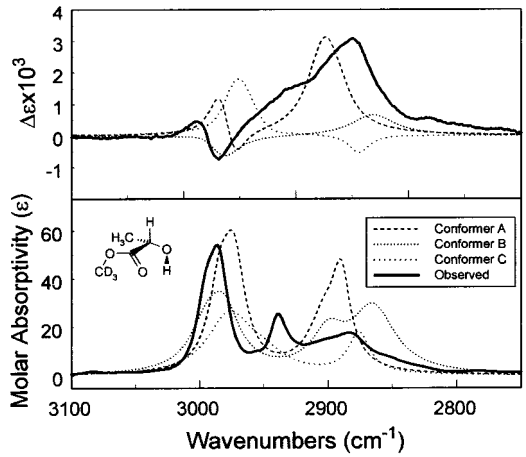

Figure 1. Comparison of experimental molar absorptivity (ϵ) and VCD ($\Delta\epsilon$) spectra of (*S*)-methyl-d_3 lactate (0.01 M in CCl_4, 1.0 cm path length) with calculated spectra for conformers A, B, and C. The methine stretch is assigned to the large positive VCD feature at 2880 cm^{-1}. Calculated methine stretching frequencies (scaled by 0.89): 2899 cm^{-1} (conformer A), 2861 cm^{-1} (conformer B), 2977 cm^{-1} (conformer C), 2897 cm^{-1} (conformer D, not shown).

lactate are compared to calculated spectra for conformers A, B, and C in Figure 1. The experimental VCD spectra in the OH- and CH-stretching regions are consistent with small populations of conformers B and C, in addition to the dominant conformer A, in 0.01 M CCl_4 solution.[4] The highest energy conformer D is not present at room temperature.

(*S*)-Methyl Lactate Methine Stretch TCD

For the TCD calculations of the methine stretch of each conformer of (*S*)-methyl-d_3 lactate-Cd_3, the molecule was aligned with the positive *z*-axis in the direction of the calculated position-form electric dipole transition moment for the methine stretch, and the same geometry, basis set, and nuclear displacement vectors employed recently for the VCD intensity calculations of this molecule were utilized here. The direction of the position-form electric dipole transition moment is used because the rotational strengths are calculated more accurately with eq 1 than with eq 10. To relate the TCD to the integrated values of the transition moments (electric dipole transition moment $(\mu)_{01}^a \equiv \mu^T$; magnetic dipole transition moment $(\mathbf{m})_{\bar{1}0} \equiv \mathbf{m}^T$), the *z*-components of the electric and magnetic dipole transition moments, and electronic and nuclear contributions to these moments ($\mu_z^T = \mu_z^N + \mu_z^E$; $\boldsymbol{m}_z^T = \boldsymbol{m}_z^N + \boldsymbol{m}_z^E$) are compiled for the four conformers in Table 1. For conformer A, the *x*-, *y*-, and *z*-components of these moments are presented in Table 2. Because μ^T lies along the *z*-direction, $\mu_x^T = \mu_y^T = 0$, $(\mu)_{01}^a = \mu_z^T$, and only $\boldsymbol{m}_z^T$ contributes to the rotational strength $R = \mathrm{Im}(\mu)_{01} \cdot (\mathbf{m})_{10}$. Thus, for this orientation, we need consider only angular and circular charge motion in the *xy*-plane to understand the origin of $\boldsymbol{m}_z^T$ and linear charge motion perpendicular to this plane to understand the origin of μ_z^T.

TABLE 2: Calculated Electric Dipole (μ) and Magnetic Dipole (m) Transition Moment Contributions for the Methine Elongation in Methyl-d_3 Lactate-Cd_3 Conformer A

component	nuclear	electronic	total
μ_x	0.079	−0.079	0.000
μ_y	0.123	−0.123	0.000
μ_z	−0.447	0.612	0.165
m_x	−0.677	0.900	0.223
m_y	0.705	−0.930	−0.225
m_z	0.088	−0.003	0.085

For this study, the TCD vectors and nuclear velocity vectors have been displayed to depict the flow of positive current for a particular phase of nuclear motion, whereas in a previous publication[10] we plotted vectors showing the direction of electron motion, opposite to the direction of positive electron current. Viewing positive electron current allows direct use of the right-hand rule via eq 12 to obtain the direction of the electronic contribution $\boldsymbol{m}_z^E$. The TCD grids contained 30 000 to 57 000 points at 0.15 Å intervals encompassing each conformer. From 3-dimensional plots of the TCD (not shown), we find that although the nuclear motion is largely isolated on the methine C*H atoms, the electronic motion is concentrated in the vicinity of the C*H bond, but is distributed throughout the entire molecule.

In Figure 2b, the TCD vectors for conformer A have been summed over the grid points in the *z*-direction and are displayed as projections in the *xy*-plane. The projected TCD-vector sums for the *xz*- and *yz*-planes of conformer A are displayed in Figure 2, c and d, respectively. The unit of length of the TCD plotted in the figures is velocity per unit volume. The largest TCD magnitudes for these three summed plots are approximately $\sim 2 \times 10^4$ m s^{-1} Å^{-3}. For this phase of vibration (methine elongation), the electric dipole transition moment, μ^T, is directed along +*z*, into the page of Figure 2a,b, whereas hydrogen motion is up, out of the page of these figures. The nuclear motion is almost completely confined to the C*H bond, and the nuclear contribution to the electric dipole transition moment, μ^N, is aligned with the methine hydrogen displacement. However, the net moment μ^T does not lie along the C*H bond and is roughly opposite in direction to the hydrogen displacement because of the 175° angle between the electronic (μ^E) and nuclear (μ^N) contributions to μ^T, and the slightly larger magnitude of μ^E compared to μ^N, as shown in Figure 3. The projected TCD sums in the *xz*- and *yz*-planes in Figure 2c,d clearly reveal a concentration of linear electronic TCD generally opposite in direction to the hydrogen displacement, but off the C*H-bond axis, which explains why the nuclear and electronic contributions to μ^T are not perfectly antiparallel. As a consequence of this linear electronic TCD that does not follow the nuclear displace-

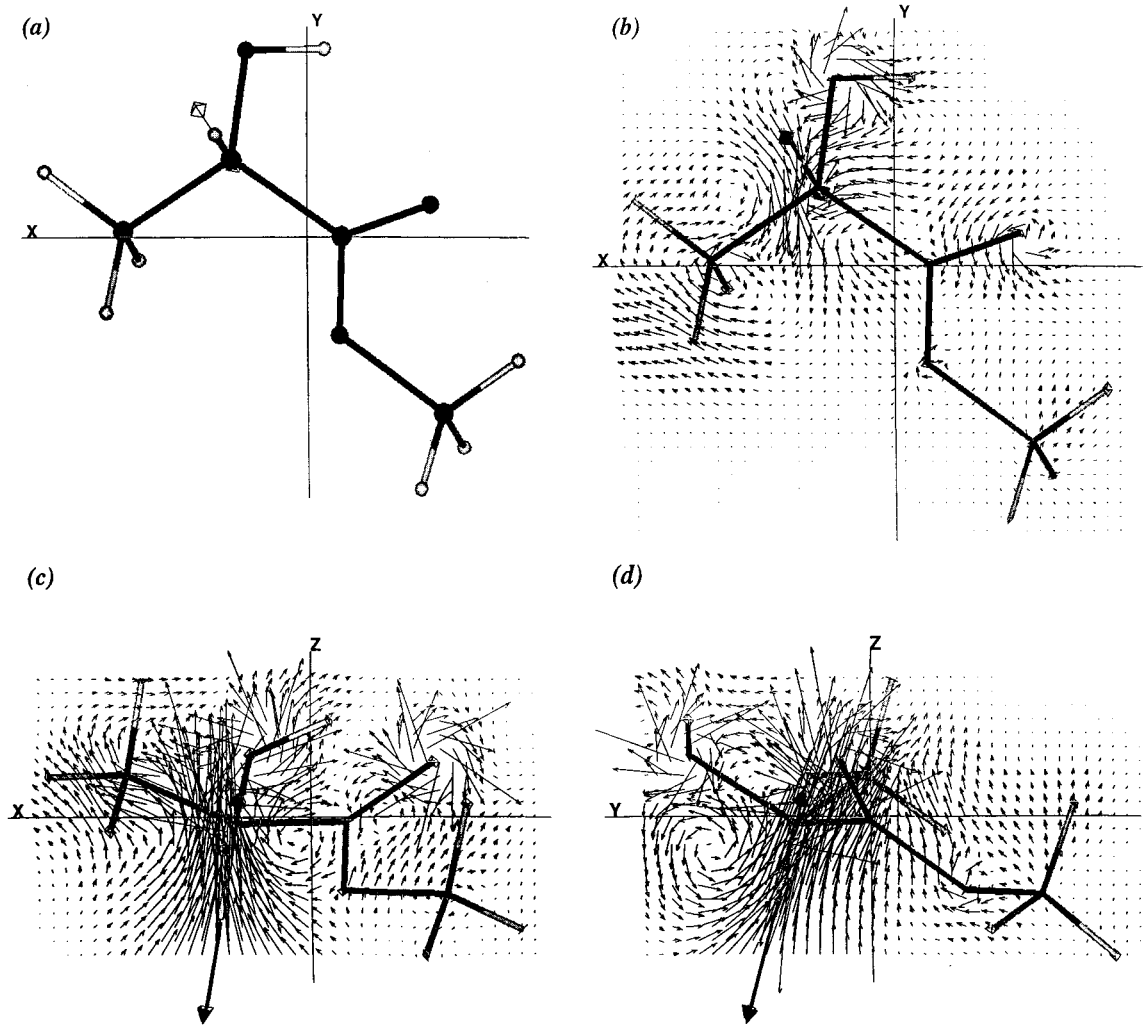

Figure 2. Methine elongation of (*S*)-methyl-d_3 lactate-Cd_3, conformer A, with origin at center of mass and *z*-axis along μ^T, showing charge-weighted nuclear displacement vectors (a) and vibrational TCD vector field, 38 × 39 × 21 point grid summed over grid points in the *z*-direction and projected in the *xy*-plane (b), summed over grid points in the *y*-direction and projected in the *xz*-plane (c), and summed over grid points in the *x*-direction and projected in the *yz*-plane (d).

ment, small components of the methine hydrogen and carbon nuclear velocity vectors lie in the *xy*-plane (Figure 2a).

Since $(\mu)_{01} = \mu_z^T$, we need only consider the magnetic dipole moment component $\boldsymbol{m}_z^T = \boldsymbol{m}_z^N + \boldsymbol{m}_z^E$ to understand the origin of the VCD intensity for this mode. We can use the right-hand rule for positive current flow to deduce contributions to $\boldsymbol{m}_z^T$ from the circular and angular charge motion viewed in the *xy*-plane projection. The nuclear contribution $\boldsymbol{m}_z^N$ is obtained by taking the vector cross product of a moment arm from the molecular origin (at the center of mass) to each nucleus with the charge-weighted nuclear velocity vector for that nucleus. Since the charge-weighted methine hydrogen velocity (or displacement) is twice as large as that for the methine carbon, the net nuclear current in the *xy*-plane has a clockwise sense of circulation about the center of mass for the view shown in Figure 2a, and the nuclear contribution $\boldsymbol{m}_z^N$ lies along $+z$. By contrast, if the nuclear displacement vectors for hydrogen and carbon were purely along the transition moment direction *z*, there could be no nuclear contribution to m_z and hence to R.

For the electronic contribution $\boldsymbol{m}_z^E$, the TCD map (Figure 2b) reveals clear patterns of angular and circular electron charge-flow. An overall pattern of clockwise charge circulation is apparent in the region of the C*CD_3 group, as well as large local clockwise circulation about the OH oxygen and small clockwise circulation about the OCD_3 oxygen. However, opposite, counterclockwise charge circulation is also present, both encompassing the bond between the methine and ester carbon atoms and as local circulation about the carbonyl oxygen. These regions of clockwise and counterclockwise circulation lead to electronic magnetic−dipole transition moment contributions to $\boldsymbol{m}_z^E$ in opposite directions. The net effect of the angular and circular TCD for this conformer is a very small electronic contribution to the magnetic dipole transition moment $\boldsymbol{m}_z^T$ (Tables 1 and 2). In this case, the large positive VCD intensity for the methine stretch results primarily from the nuclear contribution to $(m)_{10}$, which has a component $\boldsymbol{m}_z^N$ parallel to μ^T (positive *z*-direction). The angular and circular electronic TCD in the *xz*- and *yz*-planes (Figure 2c and 2d) do not contribute to the VCD intensity, since there are no components of μ^T perpendicular to these planes (Table 2).

The TCD vectors summed along the direction of the electric−dipole transition moment (*xy*-plane projections) for the methine elongations of conformers A, B, C, and D are compared in Figure 4. In contrast to the regions of opposing charge circulation for conformer A (Figure 4a), for conformer B (Figure 4b), there is local counterclockwise charge circulation about all three oxygen atomic centers and about the methine carbon. There are no distinct regions of clockwise electronic TCD flow.

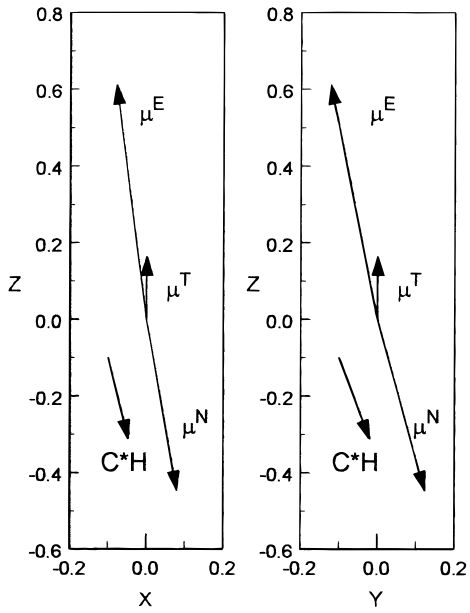

Figure 3. Electronic contribution (μ^E), nuclear contribution (μ^N) and total (μ^T) electric dipole transition moment for the methine elongation of (*S*)-methyl-d_3 lactate-Cd_3, conformer A, projected in the *xz*- and *yz*-planes and compared to the direction of the methine (C*H) displacement.

For conformer B, the component m_z^E lies in the negative *z*-direction and nearly cancels the nuclear contribution $\boldsymbol{m}_z^N$ (Table 1); the total magnetic dipole transition moment in the *z*-direction for conformer B is much smaller than that for conformer A, and much weaker rotational strength is calculated.

For the methine elongation of conformer C, counterclockwise local TCD circulation about the carbonyl and OCD_3 oxygen and methine carbon centers is observed in the projected TCD sum in Figure 4c. For this conformer, opposing clockwise circulation is encountered at the α-methyl carbon, and the more extended counterclockwise flow emanating from the carbonyl group in conformer B is absent in conformer C. Both the net electronic and nuclear contributions to $\boldsymbol{m}_z^T$ are smaller for C, compared to B. The total $\boldsymbol{m}_z^T$ component is positive (Table 1), and intermediate in magnitude between those of conformers A and B. The calculated rotational strength for C is half that of A; since the dipole strength is also smaller than that for A, the anisotropy ratios for the methine stretches of A and C are similar.

The projected TCD vector sums for conformer D are shown in Figure 4d. This conformer differs from conformer A by 180° rotation of the hydroxyl group. With this conformational change, comparing Figure 4, a and d, reveals that the sense of TCD circulation about the hydroxyl oxygen center remains clockwise, but the circulation about the carbonyl and OCD_3 oxygens is reversed. Counterclockwise angular flow is observed across the C−C*−C bonds. The net sense of flow is counterclockwise, with less cancellation than in conformer A, leading to an $\boldsymbol{m}_z^E$ contribution in the negative *z*-direction. The rotational strength and anisotropy ratio for the methine stretch in conformer D are calculated to be about 60% of the values for conformer A.

Discussion

The TCD plots for the methine stretch in the four conformers of (*S*)-methyl-d_3 lactate-Cd_3 provide visualization of the interplay between electronic and nuclear contributions to electric and magnetic dipole transition moments and of the origin of the infrared absorption and VCD intensity for this mode. The nuclear contribution to the electric dipole transition moment, μ^N, lies along the direction of the methine hydrogen displacement, and the localized, uncoupled methine stretch would generate no VCD intensity if the electronic motion perfectly followed the nuclear motion. The concentration of TCD vectors near, but at a slight angle to, the methine hydrogen displacement, as well as electronic TCD dispersed throughout the rest of the molecule (Figure 2c,d) explains the orientation of the electronic contribution to μ^T. In terms of electron density displacement (opposite to the direction of positive electron current shown in the figures), the methine stretch pulls electron density generally in the direction of the predominant hydrogen displacement as expected, but the effect of nuclear displacement on the electron density is dispersed throughout the molecule. Because of the larger magnitude of μ^E compared to μ^N, the angle between the hydrogen displacement and the total electric dipole transition moment μ^T is between 162° and 170° for conformers A−D.

Although the rotational strength for exact wave functions is origin independent, and the origin dependence of the rotational strength for approximate wave functions can be reduced by utilizing a distributed origin gauge[23,35] or eliminated by use of gauge-independent atomic orbitals[26,35] in the calculation of the magnetic dipole transition moment, the magnetic dipole transition moment itself is origin dependent. For each conformer, the origin employed for our VCD calculation is the center of mass. The angular and circular TCD patterns can be used to deduce the sign of the electronic contribution $\boldsymbol{m}_z^E$ through visualization of these patterns by taking moment arms from the center of mass as the origin for the angular charge circulation across groups of atoms (origin dependent), and circular TCD patterns with moment arms from the atomic centers (origin independent). The origin dependent process corresponds to visual integration of the type $\mathbf{R}_i^0 \times (\partial\vec{\mu}_v^i/\partial P_a)_0$ (cf. eq 10) or $\boldsymbol{R}_i^0 \times \{\boldsymbol{J}_{g0,g1}^a(\boldsymbol{r})\}^i$ (cf. eq 13), that is, taking the vector cross product utilizing moment arms from the origin at the center of mass to regions of linear TCD flow, and visually summing the contributions. The origin-independent contributions are associated with intrinsic $(\partial\vec{m}_{loc}^B/\partial P_a)0$ (eq 10) or $\boldsymbol{r}_i \times \{\boldsymbol{J}_{g0,g1}^a(\mathbf{r})\}^i$ (eq 13) contributions for local circular charge flow and an origin at the atomic nucleus. The sign of the nuclear contribution is deduced by considering a moment arm from the center of mass to the charge-weighted vibrational displacement vector at each atomic center.

For the four conformers of (*S*)-methyl-d_3 lactate-Cd_3, the variation in magnitude of the calculated rotational strength is related to the extent to which the oppositely signed electronic and nuclear contributions to the *z*-component m_z^T cancel: a dominance of the nuclear contribution yields the largest positive VCD (conformer A), near cancellation of the contributions results in very weak VCD (conformer B) and intermediate values of the electronic contribution produces some cancellation and positive VCD between these extremes (conformers B and C). The TCD maps in Figure 2, c and d, reveal charge circulations that also produce components of the magnetic dipole transition moment in the *xy*-plane (Table 2), but which do not contribute to the rotational strength.

The VCD intensity for the isolated methine stretch serves as a marker for configuration and conformation in a variety of chiral molecules[4,16,19] and thus the mechanism for generating the VCD for this mode is apparently quite robust. One large group of molecules for which an intense methine-stretching VCD marker band has been identified is characterized by heteroatom (X), carbonyl, and methyl or phenyl substituents at the chiral center (amino acids,[14,16] peptides,[16] α-hydroxy esters

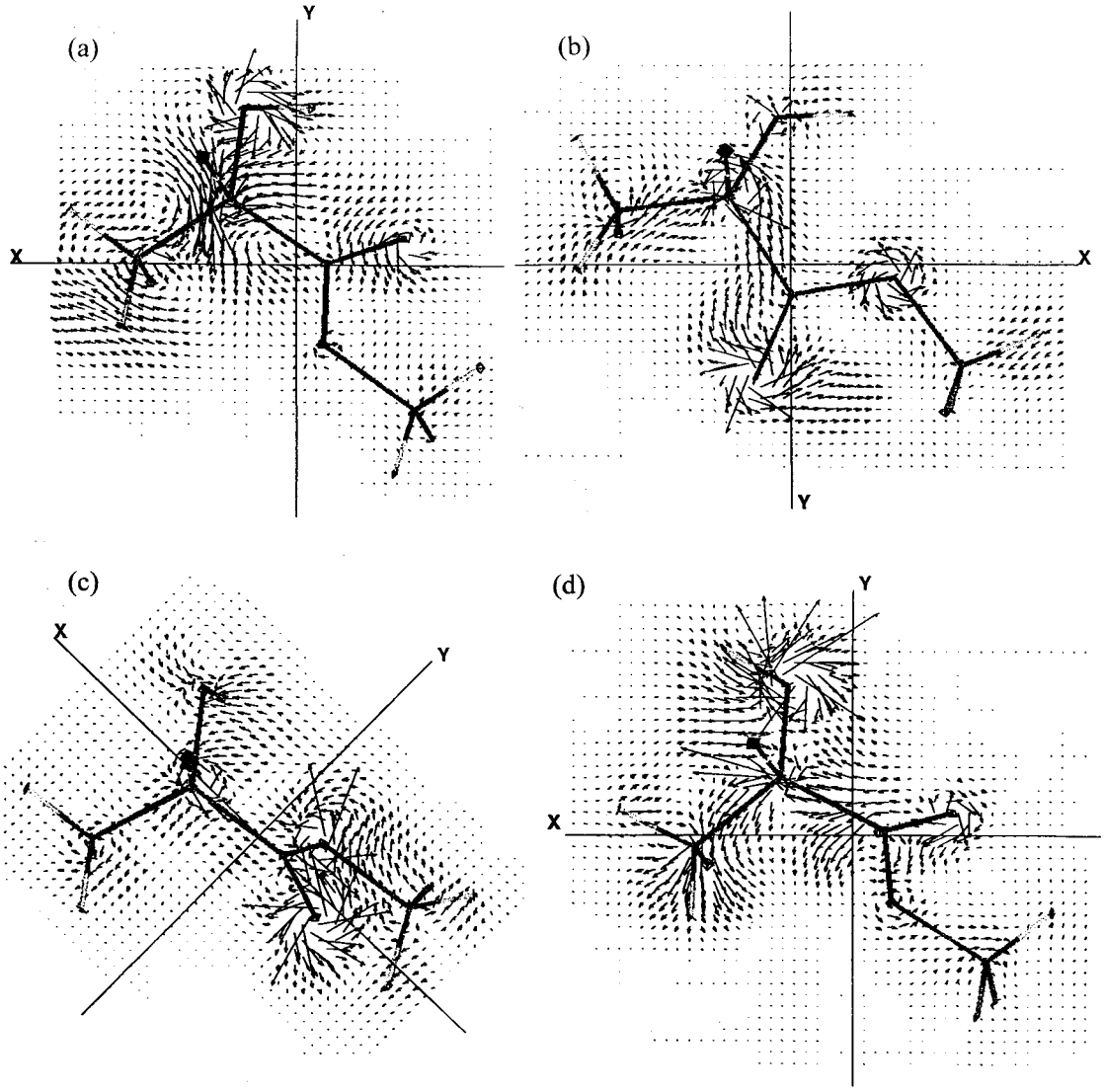

Figure 4. Vibrational TCD vector field and charge-weighted nuclear displacements for the methine elongation of (*S*)-methyl-d_3 lactate-Cd_3, summed over grid points in the *z*-direction and projected in the *xy*-plane, with origin at center of mass: (a) conformer A, 38 × 39 × 21 point grid; (b) conformer B, 47 × 36 × 20 point grid; (c) conformer C, 41 × 22 × 33 point grid; (d) conformer D, 45 × 41 × 31 point grid.

and related molecules[4]) with a cis, approximately planar X—C*—C═O arrangement. The TCD for the predominant conformer A of methyl lactate suggests that cancellation from circular charge flow patterns throughout the molecule results in a small electronic contribution, and thus a dominance of the nuclear contribution to the magnetic dipole transition moment, producing a net magnetic dipole transition moment component in the direction of the electric dipole transition moment. For the other molecules in this class, replacing the hydroxyl with an amino group or the ester with a carboxylate or phenyl ketone may not greatly alter the TCD patterns, since the hydrogen at the heteroatom and the OCD_3 group do not appear to make large TCD contributions. We are continuing calculations of the TCD for the methine stretch in L-alanine (intense positive methine-stretching VCD) and (*S*)-methyl 2-chloroproprionate (weak methine-stretching VCD) to further correlate TCD patterns with VCD intensity. For L-alanine, the methine deformations also provide examples of localized, uncoupled vibrations that give rise to characteristic VCD features. In general, we are interested in identifying the spatial origin of large VCD patterns that have been observed to be common for similar vibrations in closely related molecules. Such an understanding will provide a more intuitive sense of when large VCD can be expected and what changes in molecular structure affect such intensities. This in turn will increase the effectiveness of VCD as a probe of molecular stereochemistry.

The empirical correlation of the large methine-stretching VCD in amino acids, peptides, α-hydroxy acids, and related molecules with the presence of predominant conformers with C*XH- -O═C intramolecularly hydrogen-bonded rings (X = O or N) formed the basis of our hypothesis that vibrationally generated electron current around such rings provided a mechanism for the large VCD intensity, which was termed the ring current mechanism.[14,17−19] Calculations by Stephens and co-workers on methyl glycolate-d_1[28] and methyl lactate[27] in non-hydrogen-bonded conformations analogous to conformer D in Scheme 1, and our empirical evidence and calculations on molecules such as (*S*)-methyl-d_3 2-(methoxy-d_3)propionate,[4] which cannot form an intramolecular hydrogen-bonded ring, subsequently demonstrated that large methine stretching VCD is observed or calculated even in the absence of hydrogen-bonding. However, a common cis O═C—C*—X geometry does correlate with the large methine-stretching VCD, and the importance of angular or circular electron charge flow involving such a moiety cannot be assessed based on the integrated values of the transition moment vectors. Direct visualization of vibrational electronic

transition current density for (*S*)-methyl-d_3 lactate-Cd_3 in this study clearly reveals that there is no extended circular or angular TCD involving the entire cis O═C─C*─X─H moiety as a ring. Although the ring current mechanism has not been employed in many years, we take this opportunity to formally retract the ring-current mechanism as a simple geometric model to explain VCD intensities. The *empirical* correlation of VCD features with conformation or configuration for molecules that possess such ring conformations remains valid, but it is clear from these TCD plots that the mechanism for the VCD intensity involves more localized charge circulation in this case.

A striking and somewhat unexpected pattern of current density observed in these TCD plots is the circulation of current about atomic centers, primarily oxygen, but also carbon. These circulations occur under conditions of approximately constant electron probability density during molecular vibration, since the current feeds into itself around the atom. This pattern has been observed previously in formaldehyde,[3,10] ethylene,[10] and oxirane[12] for modes that are symmetry allowed for components of the angular momentum operator. The existence and beauty of these atomic current patterns were unknown before the implementation of vibrational TCD plots.

In understanding the origin of VCD intensity, we emphasize that it is important to consider only those circulatory current patterns that occur in planes perpendicular to the direction of the electric dipole transition moment. For our orientation, for all the conformers of (*S*)-methyl-d_3 lactate-Cd_3, the nuclear and electronic contributions to $\mathbf{m}^T$ in the *x*- and *y*-directions are much larger than the *z*-components (Table 2), and it is clear from Figure 2c,d that large charge circulations take place in the *yz*- and *xz*-planes that are largely perpendicular to the hydrogen-bonded ring. However, only the component of $\mathbf{m}^T$ in the direction of the electric dipole transition moment contributes to the rotational strength, in our case the *z*-direction, which is almost perpendicular to the ring. Vibrational circular dichroism is a small effect, and this study of vibrational TCD reveals that even relatively large VCD signals arise from a delicate balance of nuclear and electronic linear and circular charge motion.

Acknowledgment. The authors acknowledge support of this work from the National Institutes of Health (GM-23567) and the New York State Center for Advanced Technology in Computer Applications and Software Engineering at Syracuse University.

References and Notes

(1) Freedman, T. B.; Nafie, L. A. In *Modern Nonlinear Optics, Part 3*; Evans, M., Kielich, S., Eds.; John Wiley & Sons: New York, 1994; Vol. 85, pp 207−263.

(2) Yang, D.; Rauk, A. In *Reviews in Computational Chemistry*; Lipkowitz, K. B., Boyd, D. B., Eds.; VCH Publishers: New York, 1996; Vol. 7, pp 261−301.

(3) Nafie, L. A. *Annu. Rev. Phys. Chem.* **1997**, *48*, 357−386.

(4) Gigante, D. M. P.; Long, F.; Bodack, L.; Evans, J. M.; Kallmerten, J.; Nafie, L. A.; Freedman, T. B. *J. Phys. Chem. A* **1999**, *103*, 1523−1537.

(5) Ashvar, C. S.; Stephens, P. J.; Eggimann, T.; Wieser, H. *Tetrahedron Asymmetry* **1998**, *9*, 1107−1110.

(6) Devlin, F. J.; Stephens, P. J.; Cheeseman, J. R.; Frisch, M. J. *J. Phys. Chem. A* **1997**, *101*, 274−283.

(7) McCann, J. L.; Rauk, A.; Wieser, H. *Can. J. Chem.* **1998**, *76*, 274−283.

(8) Nafie, L. A. *J. Phys. Chem. A* **1997**, *101*, 7826−7833.

(9) Freedman, T. B.; Gao, X.; Shih, M.-L.; Nafie, L. A. *J. Phys. Chem. A* **1998**, *102*, 3352−3357.

(10) Freedman, T. B.; Shih, M.-L.; Lee, E.; Nafie, L. A. *J. Am. Chem. Soc.* **1997**, *119*, 10620−10626.

(11) Nafie, L. A. In *Molecular and Biomolecular Electronics*; Birge, R. R., Ed.; American Chemical Society: Washington, DC, 1994; Vol. 240, pp 63−80.

(12) Freedman, T. B.; Lee, E.; Nafie, L. A. *J. Mol. Struct.*, in press.

(13) Stephens, P. J.; Devlin, F. J.; Ashvar, C. S.; Chabalowski, C. F.; Frisch, M. J. *Faraday Discuss.* **1994**, 103−119.

(14) Nafie, L. A.; Oboodi, M. R.; Freedman, T. B. *J. Am. Chem. Soc.* **1983**, *105*, 7449−7450.

(15) Oboodi, M. R.; Lal, B. B.; Young, D. A.; Freedman, T. B.; Nafie, L. A. *J. Am. Chem. Soc.* **1985**, *107*, 1547−1556.

(16) Zuk, W. M.; Freedman, T. B.; Nafie, L. A. *J. Phys. Chem.* **1989**, *93*, 1771−1779.

(17) Freedman, T. B.; Balukjian, G. A.; Nafie, L. A. *J. Am. Chem. Soc.* **1985**, *107*, 6213−6222.

(18) Nafie, L. A.; Freedman, T. B. *J. Phys. Chem.* **1986**, *90*, 763−767.

(19) Freedman, T. B.; Nafie, L. A. In *Topics in Stereochemistry*; Eliel, E. L., Wilen, S. H., Eds.; John Wiley & Sons: New York, 1987; Vol. 17, pp 113−206.

(20) Nafie, L. A.; Freedman, T. B. *J. Chem. Phys.* **1983**, *78*, 7108−7116.

(21) Nafie, L. A. *J. Chem. Phys.* **1983**, *79*, 4950−4957.

(22) Stephens, P. J. *J. Phys. Chem.* **1985**, *89*, 748−752.

(23) Stephens, P. J. *J. Phys. Chem.* **1987**, *91*, 1712.

(24) Buckingham, A. D.; Fowler, P. W.; Galwas, P. A. *Chem. Phys.* **1987**, *112*, 1−14.

(25) Yang, D.; Rauk, A. *J. Chem. Phys.* **1992**, *97* (9), 6517−6534.

(26) Cheeseman, J. R.; Frisch, M. J.; Devlin, F. J.; Stephens, P. J. *Chem. Phys. Lett.* **1996**, *252*, 211−220.

(27) Bursi, R.; Devlin, F. J.; Stephens, P. J. *J. Am. Chem. Soc.* **1990**, *112*, 9430−9432.

(28) Bursi, R.; Stephens, P. J. *J. Phys. Chem.* **1991**, *95*, 6447−6454.

(29) Freedman, T. B.; Nafie, L. A.; Yang, D. *Chem. Phys. Lett.* **1994**, *227*, 419−428.

(30) Frisch, M. J.; Trucks, G. W.; Head-Gordon, M.; Gill, P. M. W.; Wong, M. W.; Foresman, J. B.; Johnson, B. G.; Schlegel, H. B.; Robb, M. A.; Replogle, E. S.; Gomperts, R.; Andres, J. L.; Raghavachari, K.; Binkley, J. S.; Gonzalez, C.; Martin, R. L.; Fox, D. J.; Defrees, D. J.; Baker, J.; Stewart, J. J. P.; Pople, J. A. *Gaussian 92*, Revision C; Gaussian, Inc.: Pittsburgh, PA, 1992.

(31) Frisch, M. J.; Trucks, G. W.; Schlegel, H. B.; Gill, P. M. W.; Johnson, B. G.; Robb, M. A.; Cheeseman, J. R.; Keith, T.; Petersson, G. A.; Montgomery, J. A.; Raghavachari, K.; Al-Laham, M. A.; Zakrzewski, V. G.; Ortiz, J. V.; Foresman, J. B.; Peng, C. Y.; Ayala, P. Y.; Chen, W.; Wong, M. W.; Andres, J. L.; Replogle, E. S.; Gomperts, R.; Martin, R. L.; Fox, D. J.; Binkley, J. S.; Defrees, D. J.; Baker, J.; Stewart, J. P.; Head-Gordon, M.; Gonzalez, C.; Pople, J. A. *Gaussian 94*, B.3 ed.; Gaussian, Inc.: Pittsburgh, PA, 1995.

(32) Frisch, M. J.; Trucks, G. W.; Schlegel, H. B.; Scuseria, G. E.; Robb, M. A.; Cheeseman, J. R.; Zakrzewski, V. G.; Montgomery, J. A., Jr.; Stratmann, R. E.; Burant, J. C.; Dapprich, S.; Millam, J. M.; Daniels, A. D.; Kudin, K. N.; Strain, M. C.; Farkas, O.; Tomasi, J.; Barone, V.; Cossi, M.; Cammi, R.; Mennucci, B.; Pomelli, C.; Adamo, C.; Clifford, S.; Ochterski, J.; Petersson, G. A.; Ayala, P. Y.; Cui, Q.; Morokuma, K.; Malick, D. K.; Rabuck, A. D.; Raghavachari, K.; Foresman, J. B.; Cioslowski, J.; Ortiz, J. V.; Stefanov, B. B.; Liu, G.; Liashenko, A.; Piskorz, P.; Komaromi, I.; Gomperts, R.; Martin, R. L.; Fox, D. J.; Keith, T.; Al-Laham, M. A.; Peng, C. Y.; Nanayakkara, A.; Gonzalez, C.; Challacombe, M.; Gill, P. M. W.; Johnson, B.; Chen, W.; Wong, M. W.; Andres, J. L.; Gonzalez, C.; Head-Gordon, M.; Replogle, E. S.; Pople, J. A. *Gaussian 98*, A.5 ed.; Gaussian, Inc.: Pittsburgh, PA, 1998.

(33) Rauk, A.; Yang, D. *J. Phys. Chem.* **1992**, *96*, 437−446.

(34) Ashvar, C. S.; Stephens, P. J.; Eggimann, T.; Wieser, H. *Tetrahedron: Asymmetry* **1998**, *9*, 1107−1110.

(35) Nafie, L. A. *J. Chem. Phys.* **1992**, *96*, 5687−5702.